

# Annealing of drawn monofilaments of liquid crystalline polymer vectra/vapor grown carbon fiber nanocomposites

Estelle Kalfon-Cohen<sup>a,\*</sup>, Alessandro Pegoretti<sup>b</sup>, Gad Marom<sup>a</sup>

<sup>a</sup> Casali Institute of Applied Chemistry, The Hebrew University of Jerusalem, 91904 Jerusalem, Israel

<sup>b</sup> Department of Materials Engineering and Industrial Technologies, University of Trento, Via Mesiano 77, 38123, Italy

## ARTICLE INFO

### Article history:

Received 8 September 2009

Received in revised form

21 December 2009

Accepted 5 January 2010

Available online 18 January 2010

### Keywords:

Thermotropic liquid crystal

Annealing

Sequence ordering

## ABSTRACT

The annealing treatment of drawn LCP nanocomposite monofilaments is discussed here. Upon annealing, an unstable structure is generated which presents a strong dependence on the annealing time sequence and temperature as observed by DSC. Moreover, it seems that increasing the draw down of the fiber restricts the formation of this new (unstable) structure. Based on dynamic mechanical analysis and on solid state <sup>13</sup>C NMR, the nature of the newly-formed structure is elucidated, and based on sequence ordering within the non-oriented amorphous phase in the copolymer, a 10% change in the monomer proportion in the ordered phase is observed after annealing.

© 2010 Elsevier Ltd. All rights reserved.

## 1. Introduction

The crystallization processes of polymers vary greatly depending on the type of polymer. Liquid crystalline polymers (LCP) generally crystallize from an ordered and oriented molecular phase. The specific rod-like structure of the liquid crystalline polymers is responsible for the oriented phase merging in the melt, but is also responsible for the resulting high melting temperature, rendering their processability difficult [1]. Addition of a comonomer disturbs the rigid register and consequently reduces the melting transition temperature [2]. Copolymers, consisting of crystallizable and non-crystallizable units, may crystallize rapidly even if the non-crystallizable units are rejected from the crystallizable regions.

Several crystallization theories for nematic random copolymers have been proposed in the past. The first model, developed by Hanna et al. [3], proposed a crystallization process based on sequence matching and segregation in adjacent chains to form three distinct regions: a crystalline-core in which the sequences in adjacent chains matched well, a partially-ordered fringe region in which sequence matching decays, and finally a non-crystalline region. The ordered entities were termed as nonperiodic layer (NPL) crystals. The second model was proposed by Biswas and Blackwell. It differs from the NPL model in that they considered an assembly of chains with random sequences as one-dimensional paracrystalline lattices

(PCLs) along the chain axis with conformational order (such as persistence length) giving rise to a “segregated chain conformation” but without sequence matching [4,5].

Annealing of a random copolymer was shown to be extremely sensitive to the annealing conditions, in particular to the annealing temperature. According to the annealing conditions an endotherm emerged at temperatures below the annealing temperature. Economy et al. [6] show that upon annealing at temperatures higher than the crystal-to-nematic transition ( $T_{CN}$ ) a chemical randomization occurs through transesterification. When annealing is performed at 10 °C below  $T_{CN}$ , an increase of alternating copolymer sequences occurs via inter-chain transesterification, thus increasing the  $T_{CN}$ . Below the  $T_{CN}$  temperature, a physical reorganization of the chain into larger segregated regions is supposed to occur at 40–50 °C below  $T_{CN}$ . According to Gentzler et al. annealing above a critical temperature induces a slow crystallization process in which solidification of higher persistence lengths takes place [7]. With regard to the mechanical properties, the effect of annealing was evaluated by Sarlin et al. [8,9], who showed that isothermal annealing at 246 °C has a positive effect on the tensile strength (30%) and on the modulus (10%). Moreover, after annealing at 270 °C for 72 h the tensile strength was improved by 160% and the modulus by 30%.

As stated, annealing of the copolyesters slightly below their crystal–nematic transition largely increases the melting point [10], for which several interpretations have been proposed [11]. One interesting proposal is sequence ordering through a process classified as crystallization induced reactions (CIR) by Lenz and coworkers [12–17], as recently confirmed conclusively by Economy et al. [6]. In

\* Corresponding author.

E-mail address: [estelle.kalfon@mail.huji.ac.il](mailto:estelle.kalfon@mail.huji.ac.il) (E. Kalfon-Cohen).

the CIR process, the initial non-crystalline random copolyester is converted to a block copolymer via ester interchange reactions in the solid state. In such a process the non-crystallizable unit sequence are replaced by crystallizable regions and thus increasing the crystal size, the crystallinity and the melting point. Moreover, it is also well-known that annealing near  $T_{CN}$  increases the molecular weight of the polymer via transesterification. For instance, heat treatment at 10–20 °C below  $T_{CN}$  in an inert environment results in improved tenacity, chemical resistance, melting point, elongation and tensile properties [18]. It has also been demonstrated that annealing at 10–30 °C under  $T_{CN}$  and under low pressure leads to a further increase of the molecular weight [19].

When annealing is performed well below  $T_{CN}$ , the CIR process requires a catalyst such as sodium acetate and/or long dwelling periods [13,14]. It was demonstrated by Lenz [12] that decreasing the molecular weight of the polymer is equivalent to increasing the concentration of polymer chain endgroups, which results in increasing the rate of the CIR reactions [16].

In our previous studies we thoroughly investigated the crystalline structure of the vectra nanocomposite and its nematic state by using an in-situ synchrotron microbeam. We showed that the addition of vapor grown carbon fibers (VGCF) which are acicular nanoparticles (with a specific high aspect ratio) allows a positive anchoring effect, reflected in a high order parameter ( $S = 0.92$ ) and in a more distinctive crystal-to-nematic transition [20]. As shown, annealing at high temperature under tension (isometric) improves the mechanical performances. Reinforcing the polymer with nanoparticles is expected to generate a further increase through increasing the crystalline proportion and order in the polymer. Indeed, Yudin et al. showed that upon isometric annealing acicular nanoparticles (VGCF) nucleate a thermoplastic polyimide and give rise to a unique orientated smectic structure that is reflected in the mechanical properties of the composite [21].

Following our previous work on vectra nanocomposites, the combined effects of draw down and annealing in a similar system are investigated here, aiming at revealing property–morphology relationship. It is noted that in the present study, a short annealing treatment was performed in the absence of catalyst in order to minimize the potential occurrence of the CIR.

## 2. Experimental

### 2.1. Materials

The thermotropic LCP used in this study is Vectra A950, Ticona. This is an aromatic copolyester composed of 1, 4-hydroxybenzoic acid (HBA) and 2, 6-hydroxynaphthanoic acid (HNA) in a molar ratio of 73/27, respectively [22]. The random copolymerization of HNA and HBA disrupts the registry between the adjacent chains thereby reducing the crystal-to-nematic transition temperature. The HNA monomer has a larger transverse size than that of the HBA monomer, which results in an increase in the inter-chain distance and a dramatic lowering of the melting temperature. Vectra A950 has a glass transition at 110 °C and a nominal crystal-to-nematic transition at 276 °C. Vapor grown carbon nanofibers VGCF-H (graphitized up to 2800 °C) were supplied by Showa Denko KK, Japan. The average diameter and length of the VGCF are 150 nm and 10–20 μm, respectively; their density is 2 g/cm<sup>3</sup>.

### 2.2. Extrusion and annealing of the monofilament

Melt mixing of Vectra A950 pellets filled with 1.5 wt% of VGCF was carried out in a twin-screw microcompounder (DSM,

Netherlands). Mixing was performed at 293 °C for a period of 10 min, according to the procedure published elsewhere [20]. This was followed by extrusion through a 900 μm die and drawing of fiber-like filaments with diameters decreasing from 900 μm to 30 μm (with corresponding draw down  $DD = 1$  to  $DD = 900$ ). The annealing process was performed in atmospheric conditions at temperatures in the range of 200–280 °C and annealing times in the range of 10–240 min.

### 2.3. Electron microscopy

The dispersion of VGCF at the tapered-section of extruded monofilaments was examined by HR-SEM (Sirion 200, FEI). The SEM samples were subjected to a chemical etching consisting of 0.7 wt%  $KMnO_4$  in a mixture of 1:2  $H_3PO_4$  and  $H_2SO_4$  [23], which preferentially attacked the amorphous matrix to reveal the crystalline structure.

To assess their orientation with drawing, TEM (Tecnai, FEI) was applied to the microtomed cross section (Ultratome III type A 8801, LKB, Sweden).

### 2.4. Thermal analysis

Differential scanning calorimetry DSC (Mettler 822e Toledo, Switzerland) thermograms were measured in the temperature range 20–400 °C at a heating rate of 10 °C/min under a nitrogen flux of 50 mL/min. The weight of each sample was approximately 10–15 mg.

### 2.5. X-ray diffraction

X-ray diffraction patterns of pristine vectran fibers were measured using a D-Max/B theta-2 theta powder diffractometer (Rigaku, Japan) in conjunction with an RU200 rotating anode X-ray generator (Rigaku) with copper target. The X-radiation was monochromatized with a graphite monochromator to an average wavelength of  $\lambda = 1.54$  Å.

The fibers were held vertical and the scan was performed in the horizontal plane.

WAXD measurements were carried out on an Elliott GX-6 rotating anode generator with copper target and operating at 12 kW.

The degree of orientation was evaluated by the order parameter  $S$  defined as [24]

$$S = 0.5 \langle (3\cos^2\theta) - 1 \rangle \quad (1)$$

where  $\theta$  is the angle between the molecular axis and the director (assumed as the filament axis) and the brackets denote an average value for many molecules.

### 2.6. Mechanical testing

Tensile testing was performed on a universal testing machine (Instron, Model 4502) at a gage length of 20 mm and loading rate of 10 mm/min. At least 10 specimens were tested for each composition and draw down.

The tensile strength was analyzed using the Weibull distribution [10]:

$$P(\sigma) = 1 - \exp\{- (\sigma/\sigma_0)^m\} \quad (2)$$

where  $P(\sigma)$  is the cumulative failure probability of a fiber at stress  $\sigma$ , while  $\sigma_0$  and  $m$  represent the scale and the shape Weibull parameter, respectively.

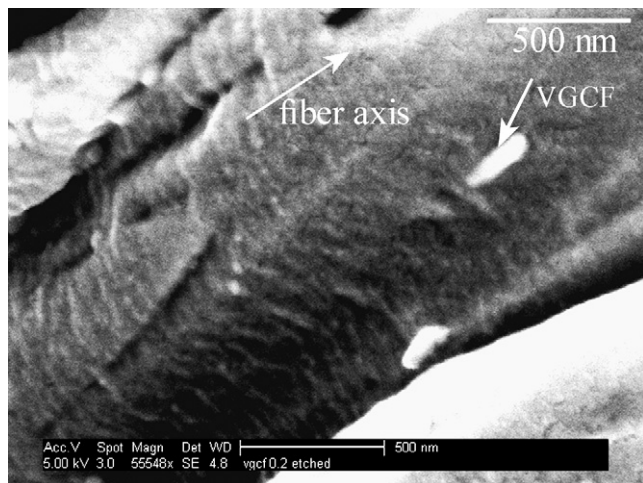


**Fig. 1.** SEM micrograph of annealed (120 min at 240 °C) vectra/VGCF monofilament at DD = 5 after etching.

### 2.7. Dynamic mechanical thermo-analysis

Tensile dynamic mechanical tests were conducted on a dynamic mechanical thermal analyzer (DMTA, model MKII, by Polymer

Laboratories Ltd, Loughborough, UK). All samples were tested at 1 Hz, in a temperature range from –100–170 °C, at a heating rate of 5 °C/min, under a constant tensile stress of 100 MPa for DD > 100 and 10 MPa for DD < 100. The specimen gage length was about 15 mm. Specimen clamping followed to ensure optimum clamping pressure at low temperature.

### 2.8. Infra-red spectroscopy

Attenuated total reflection Fourier transform infrared spectroscopy (ATR-FTIR) was carried out on an ALPHA apparatus by Bruker, Germany, in order to follow potential annealing generated chemical changes.

### 2.9. Solid state $^{13}\text{C}$ NMR

The measure of the HBA/HNA composition is the relative area of the HBA and HNA ether ring carbon peak in the  $^{13}\text{C}$  CP-MAS NMR spectra. Suitable spectra were obtained at the following conditions: an  $^1\text{H}$  90° pulse of 2.8  $\mu\text{s}$ , 50 kHz CP with a 2-m contact time and 2.8 kHz MAS spinning speed. The analysis was carried out using a Bruker DRX-400 spectrometer equipped with a BGU II z-gradient. The materials were crushed and an average weight of 20 mg was used.

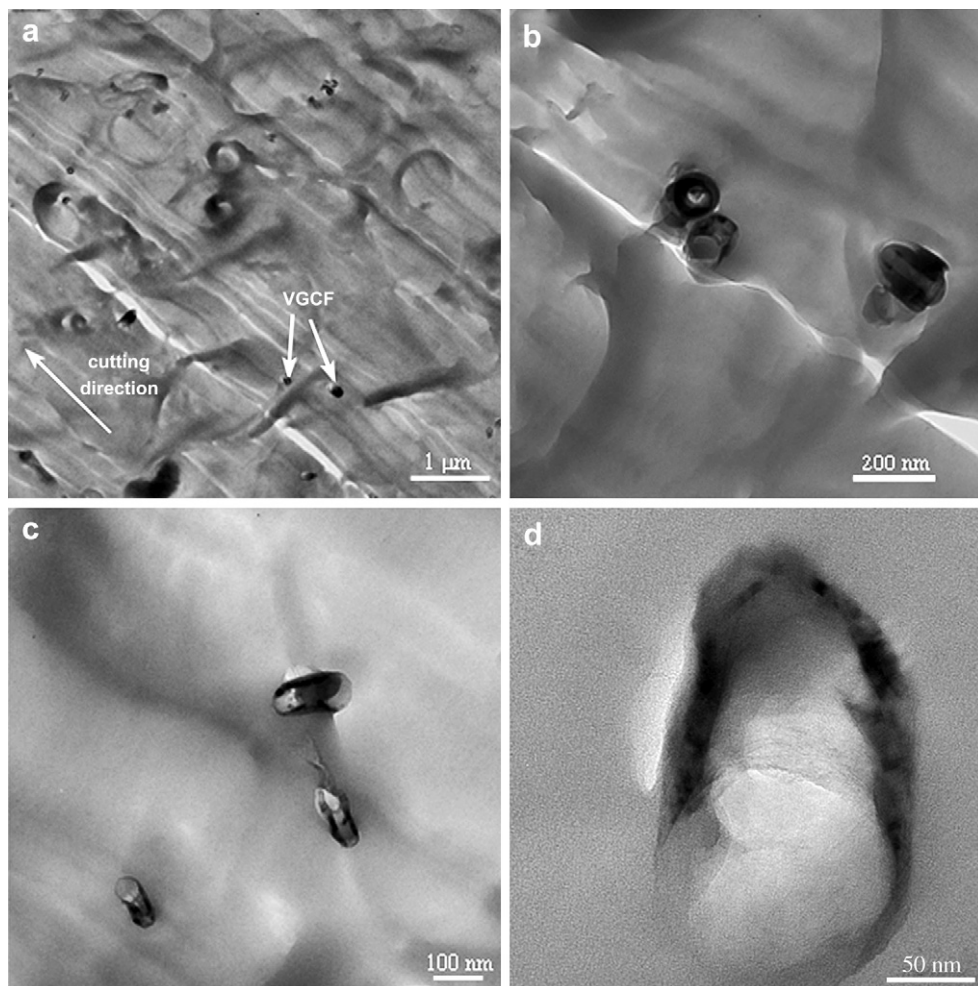


**Fig. 2.** TEM micrograph at various magnifications of a microtomed cross section vectra/VGCF monofilament after annealing 120 min at 240 °C (at DD = 5).

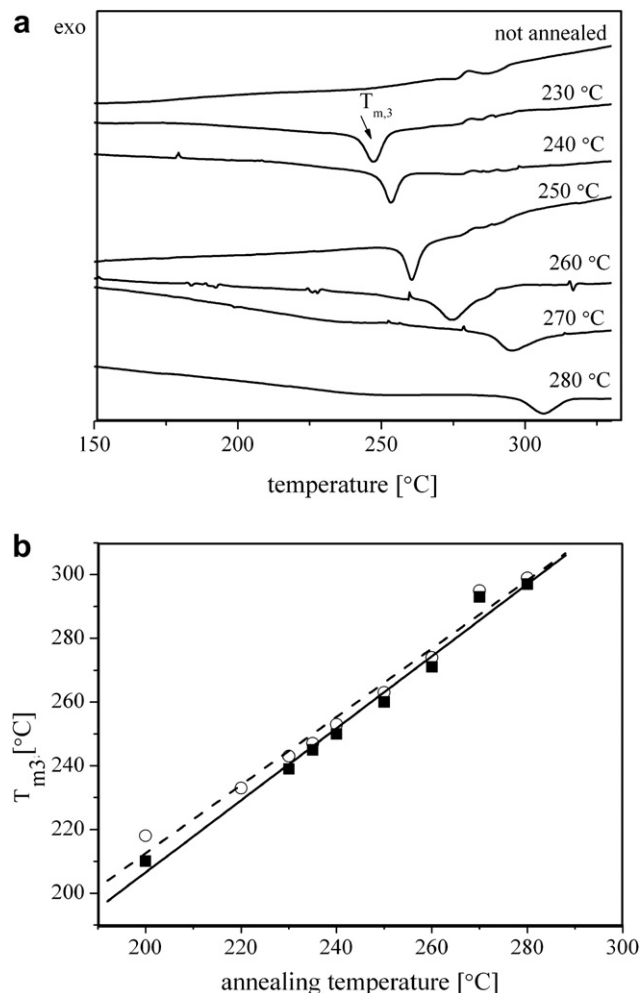


**Fig. 3.** DSC traces of (a) vectra/VGCF as a function of annealing temperature. The annealing time was 120 min. The relationship between  $T_{m3}$  and annealing temperature is represented in (b) for (—■—) vectra and (---○---) vectra/VGCF.

### 3. Results

Fig. 1 presents a tapered-section of an annealed monofilament which was frozen-sliced and then etched to reveal the crystalline structure of the polymer. First, we can note the orientation of the VGCF inclusions along the fiber axis, namely the draw direction. Moreover, the etching revealed a layer structure perpendicular to the fiber, which seems to be independent of the VGCF presence and reminiscent of the smectic morphology. TEM micrographs of the un-etched monofilament are shown in Fig. 2. The contrast in the TEM bright field image is due to sample thickness variation. Bright and dark sections indicate thin and thick regions, respectively. These are artifacts of cutting, which also resulted in the appearance of layers (black lines) perpendicular to the longitudinal direction, and are illustrated by an arrow in Fig. 2a. In Fig. 2a it is clearly

**Table 1**  
 $T_{m3}$  and corresponding enthalpy in vectra and vectra/VGCF for different draw downs. The filaments were annealed at 240 °C for 120 min.

DD	$T_{m3}$ (°C)		$\Delta H$ (J.g <sup>-1</sup> )	
	vectra	vectra/VGCF	vectra	vectra/VGCF
1.5	257	257	2.49	2.72
13	256	256	2.42	2.71
225	254	255	2.25	2.38

shown that the VGCFs are well dispersed in the polymer matrix and are well oriented along the axis direction despite the low drawing force applied during the extrusion of a DD = 5 filament. In Fig. 2b and c very thin banded structures were observed as described by [25] but no direct correlation with the presence of VGCF inclusions can be drawn.

The DSC traces of vectra/VGCF monofilament (DD = 5) are presented in Fig. 3a as a function of the annealing temperature. Before any treatment, the polymer displays two broad endotherms at 277 °C and 290 °C which were previously assigned respectively to the conversion of the orthorhombic structure fraction to a pseudo-hexagonal (PH) arrangement and to the crystal-to-nematic transition [20]. As the annealing temperature is increased, a third endotherm (called  $T_{m3}$ ) emerges at lower temperatures, i.e. at around 10 °C above the annealing temperature, and this shifts to higher temperatures as the annealing temperature is increased. Concomitantly, the transition enthalpy increases. Note that annealing the monofilaments just below the crystal-to-nematic transition leads to a merging of the peaks at 277 °C. This phenomenon has been widely covered by the literature and resulted from inter-chain transesterification reaction. The influence of VGCF addition on vectra DSC trace is shown in Fig. 3b by comparing the  $T_{m3}$  of filled and unfilled vectra at different annealing temperatures. First, addition of VGCF slightly shifts the  $T_{m3}$  to a higher temperature. For both unfilled and filled vectra, the transition temperature  $T_{m3}$  increases linearly with the annealing temperature. Moreover

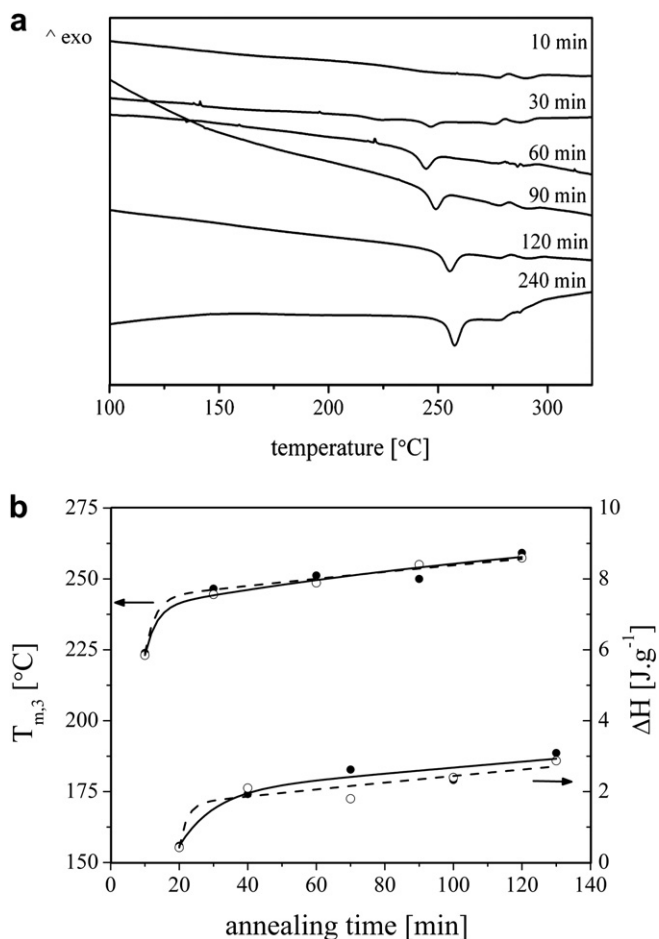


**Fig. 4.** (a) DSC traces of vectra/VGCF as a function of the annealing time. The annealing was performed at 240 °C. (b) The enthalpy released and the  $T_{m3}$  in (—●—) unfilled vectra and (---○---) filled vectra is compared as a function of the annealing time.

the corresponding enthalpy increases when VGCF are introduced, as displayed in Table 1. In the same table, we note that increasing the draw down of the monofilaments from 1 to 225 reduces the  $T_{m3}$  enthalpy by 9% in unfilled vectra and by 12% in filled vectra. In addition,  $T_{m3}$  shows a strong dependence on the annealing time as observed in Fig. 4a. The temperature of  $T_{m3}$  and its respective enthalpy increases with the annealing time when the annealing temperature is kept at 240 °C (Fig. 4b). Apparently, a structure is formed which is unstable with respect to slight changes in temperature. The stability of the structure increases with the annealing temperature. It should be noted that unlike  $T_{m3}$ , the higher transitions are independent of the annealing conditions.

The XRD diagrams of the annealed monofilaments are presented in Fig. 5a and Fig. 5b and display the structural changes occurring in vectra/VGCF for different annealing conditions. It seems that no significant recrystallization takes place during the annealing. Two intensity peaks are observed in the  $2\theta$  diagrams. The main intensity peak is observed at  $2\theta = 19^\circ$  and is assigned to the (110) plane according to the pseudo-hexagonal unit cell. A second lower intensity peak is observed at  $2\theta = 27^\circ$  and is assigned to the off-equatorial (211) plane of the same unit cell structure. Increasing the annealing conditions via higher temperatures and longer annealing times, led to an asymmetry of the (110) peaks, similar to the asymmetry observed in the high strength type of vectran identified in our previous study by the formation of an orthorhombic phase [26]. Simultaneously, the intensity of the (110) plane is unexpectedly reduced, due to reduction of the crystalline fraction. Whereas the high mechanical properties of vectra HS fibers have been attributed to a new orthorhombic phase developed during the treatment (confirmed by the appearance of the splitting of the (110) diffraction) [26–28], no evidence of annealing-related recrystallization was observed here. It should be noted that neat vectra filaments exhibited exactly the same diffraction pattern regardless of annealing and VGCF addition. This observation seems to exclude the possibility of crystallization induced reactions that would result in the formation of an orthorhombic fraction due to the recrystallization of the block copolymer.

The WAXD patterns of the vectra/VGCF monofilaments (before and after annealing) are presented in Fig. 6. Three circular diffractions are observed that correspond to the (110), the (211) and the (006) planes. After annealing the diffractions are intensified and arc-shaped, indicating a qualitative improvement of the orientation.

The effect of annealing on polymer orientation at room temperature can be evaluated qualitatively by profile fitting the azimuthal scan of the (110) reflection. Scan of unannealed and annealed filament (DD = 5) are superposed in Fig. 7a. The azimuthal full-width half-maximum decreases by approximately 70% after annealing indicating an improvement of the chain orientation. Quantitative orientation of the monofilament was evaluated by calculating the order parameter ( $S$ ) according to eq. (1). Fig. 7b shows the respective order parameter obtained for fibers of different DD before and after annealing. An increase of the order parameter is noted for low DD while at high DD it seems to be unchanged. A plausible explanation is that the original high degree of orientation developed in high DD fibers (almost 0.9) cannot be improved by further molecular motion. The considerable tensile force applied during the fiber extrusion leads to a “frozen” stretched molecular configuration, rendering any molecular motion impossible in contrast to the low drawn fiber. Similar observations were described by Kaito et al. [28]. Their explanation, however, was based on what they considered a new crystalline structure with a  $T_{m3}$  melting transition – a supposition that is rejected here on the basis of thorough crystallographic evidence.

The effect of the orientation and the crystalline structure is reflected in the mechanical properties.

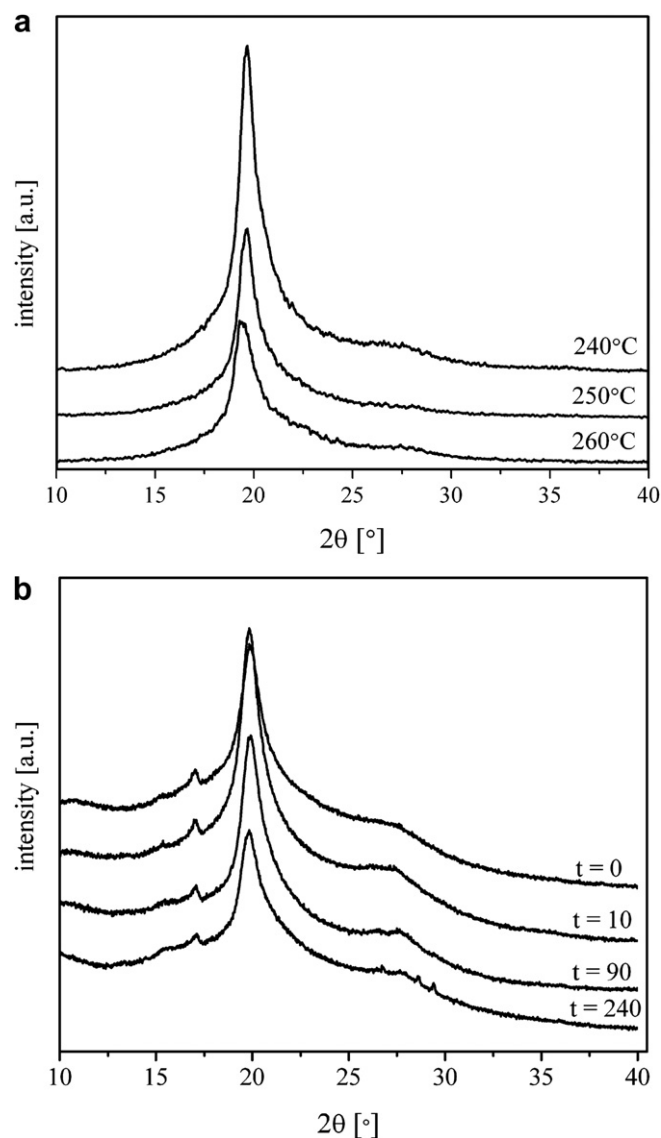


Fig. 5. XRD diagrams of vectra/VGCF monofilament (DD = 5) as a function of (a) the annealing temperature (for 120 min) and (b) the annealing time (at 240 °C).

Examples of stress-strain curves are presented in Fig. 8a and display the behavior of the monofilaments under tensile test before and after the annealing treatment. The stress at break and the strain are improved by more than 50% for DD = 225 after annealing while at low DD the monofilaments seem to break at lower stress but higher strain. It is seen that despite the fact that the behavior is controlled principally by the extent of DD, annealing produces a significant effect even for high DD levels. Fig. 8b presents the tensile modulus of the reinforced monofilament after annealing. It seems that annealing low DD vectra/VGCF monofilaments (up to DD = 100) increases the modulus by more than 100%, i.e. with growing values from 46 to 80 GPa for DD = 56. Beyond DD = 100 the trend is reversed and displays lower modulus values after annealing. The tensile strengths of the monofilaments are displayed in Fig. 8c. Weibull distribution analysis was evaluated on fifteen specimens of unannealed filaments with DD = 225 and displays scale and shape parameters  $\sigma_0 = 1553$  MPa and  $m = 6.01$  [20], respectively. The same filaments after annealing showed  $\sigma_0 = 2272$  MPa and  $m = 7.72$  for the scale and shape parameters, respectively, which represents an improvement of 30%. A

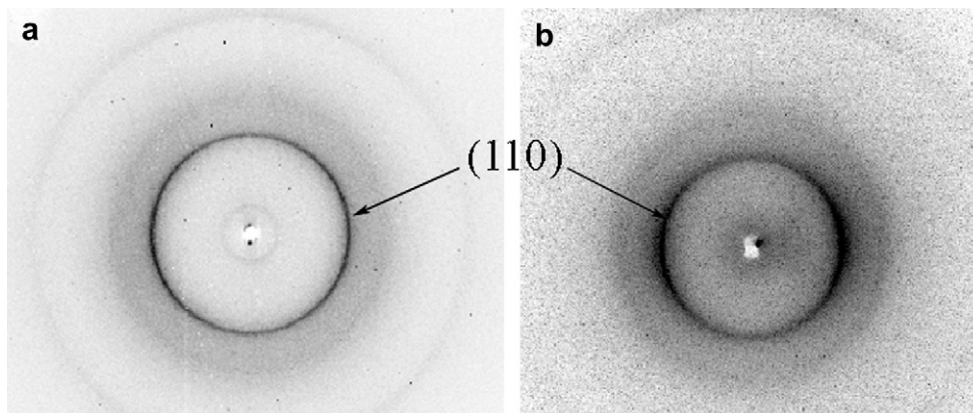


Fig. 6. 2D WAXD patterns of vectra/VGCF (a) before and (b) after annealing (120 min at 240 °C).

relationship can be drawn from the mechanical results and the morphological structure studied before.

The mechanical properties are expected to correlate with the order parameter, however, their dependences on DD varies so that the inflection point of the latter appears at different DD ratios (i.e.,

Fig. 7b vs. Fig. 8c), reflecting perhaps an orientated nematic morphology formed already at lower DD values and a quasi-smectic morphology that is produced under higher DD. The long range order is expected to improve the mechanical properties but with minimum effect on the WAXD based order parameter.

The potential occurrence of chemical reactions such as transesterification during the annealing treatment at 240 °C was further checked by ATR-FTIR measurements as shown in Fig. 9. The fact that the aryl-ester absorbance peak observed at 1739  $\text{cm}^{-1}$  remains unchanged after the annealing treatment is taken as a strong indication for the absence of any chemical reactions during annealing. Moreover, identical spectra were observed for neat vectra before and after annealing as shown in Fig. 9a. We therefore propose that the absence of CIR based chemical changes results from the employed annealing conditions (short and without catalyst) rather than from the presence of the filler.

The dynamic mechanical analysis of the monofilaments was performed under tensile test. The  $\tan \delta$  plots in Fig. 10 display three relaxation transitions, at  $-50$  °C, 30 °C and 100 °C, and are conventionally named  $\alpha$ ,  $\beta$  and  $\gamma$  in order of decreasing temperature [29]. The  $\alpha$  process is assigned to the relaxation of the overall chain and corresponds to the transition from a nematic “frozen” state to a mobile nematic phase. The  $\beta$  and  $\gamma$  processes are local mode processes associated with the C–O bond rotation in HNA and HBA, respectively [30–32]. Table 2 and Table 3 list the three transition temperatures and intensities as a function of the DD and annealing process in vectra monofilaments. Three main features are evident when comparing the different systems. The  $\alpha$  and  $\beta$  relaxations are shifted to lower temperatures as the DD is increased. Contrarily, the  $\gamma$  transition is displaced to higher temperatures. Secondly, upon annealing, all three transitions are shifted to higher temperatures. Also, the intensity of the  $\beta$  process is increased while that of the  $\alpha$  process is sharply decreased. These two phenomena occur simultaneously. Interestingly, the same features were noted previously when the amount of HNA in the copolymer was increased [33]. It should be noted that these same features were observed in unfilled monofilaments, with a slight shift of the relaxation transition to lower temperatures. The shift of the  $\beta$  and  $\gamma$  processes to higher temperatures after annealing confirms the hypothesis of reorganization, inducing a limitation of the ring rotation.

It is well-known that the high mechanical properties observed in the industrial vectran fibers result from the highly oriented structure generated from the nematic state, comprised of amorphous and crystalline fractions. During annealing the amorphous phase can reorganize if the free motion of the molecular chains is sufficient. In the case of extended rigid rod polymers, the low degree of freedom restricts the process of reorganization. In the following discussion

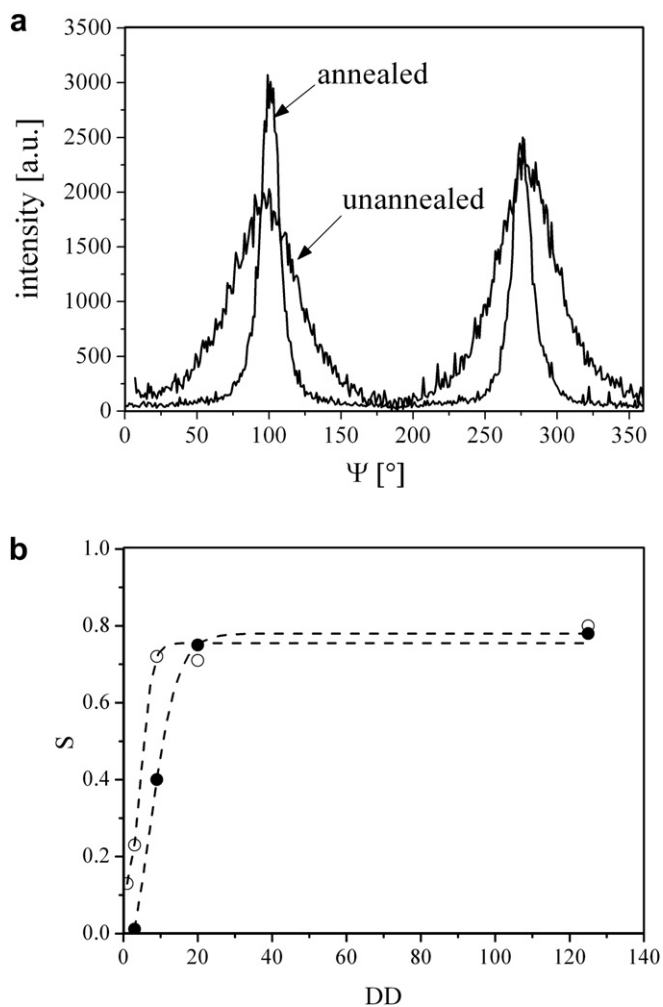
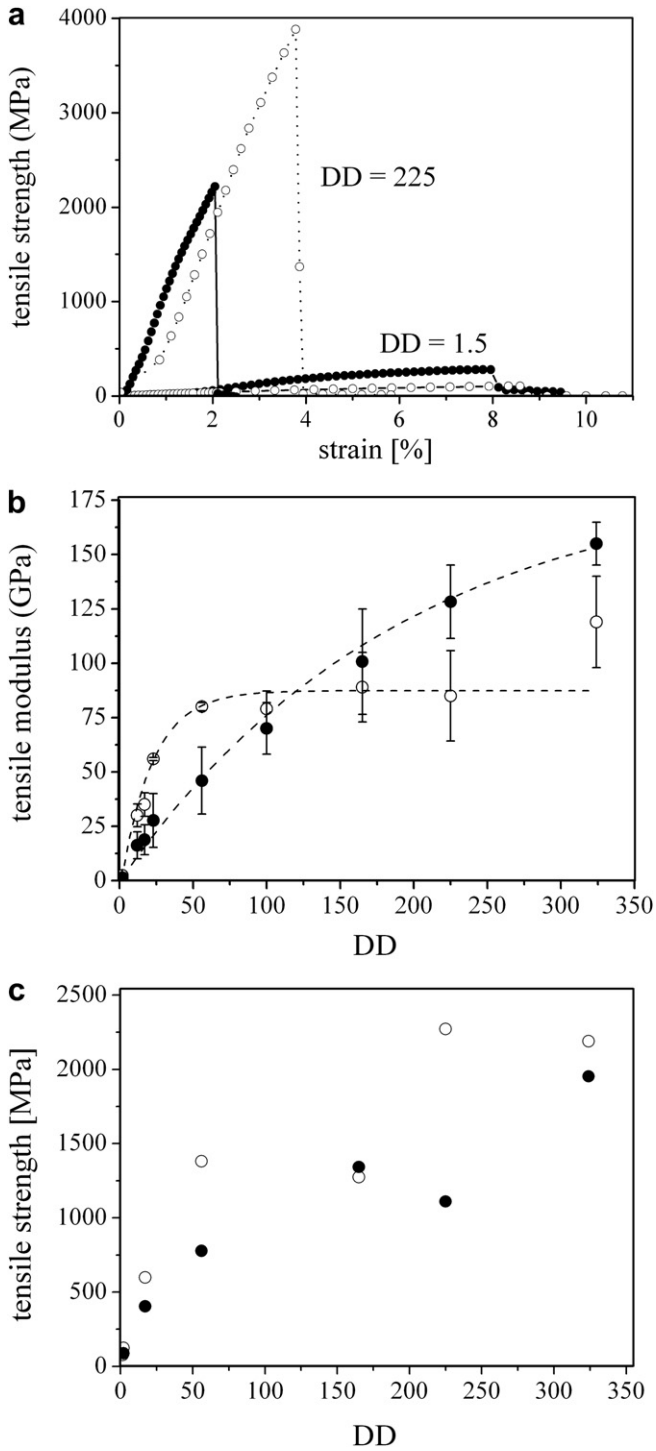


Fig. 7. (a) Azimuthal ( $\Psi$ ) scans of the (110) reflection measured at room temperature for vectra/VGCF (DD = 5) before and after annealing (120 min at 240 °C). (b) The calculated order parameters  $S$  as a function of the DD in (●) unannealed vectra/VGCF and (○) vectra/VGCF annealed 120 min at 240 °C.



**Fig. 8.** (a) Stress-strain curves, (b) tensile modulus and (c) tensile strength as a function of DD in vectra/VGCF (—●—) before and (—○—) after annealing 120 min at 240 °C. The scatter bar in Fig. 8b were added according to the standard deviation.

the effects of draw down and annealing process on the reorganization process in the vectra polymer are considered.

#### 4. Discussion

In general, the annealing of common semi-crystalline polymers above the glass transition temperature allows minimal motion of the molecular chains that tend to recrystallize into a more oriented and

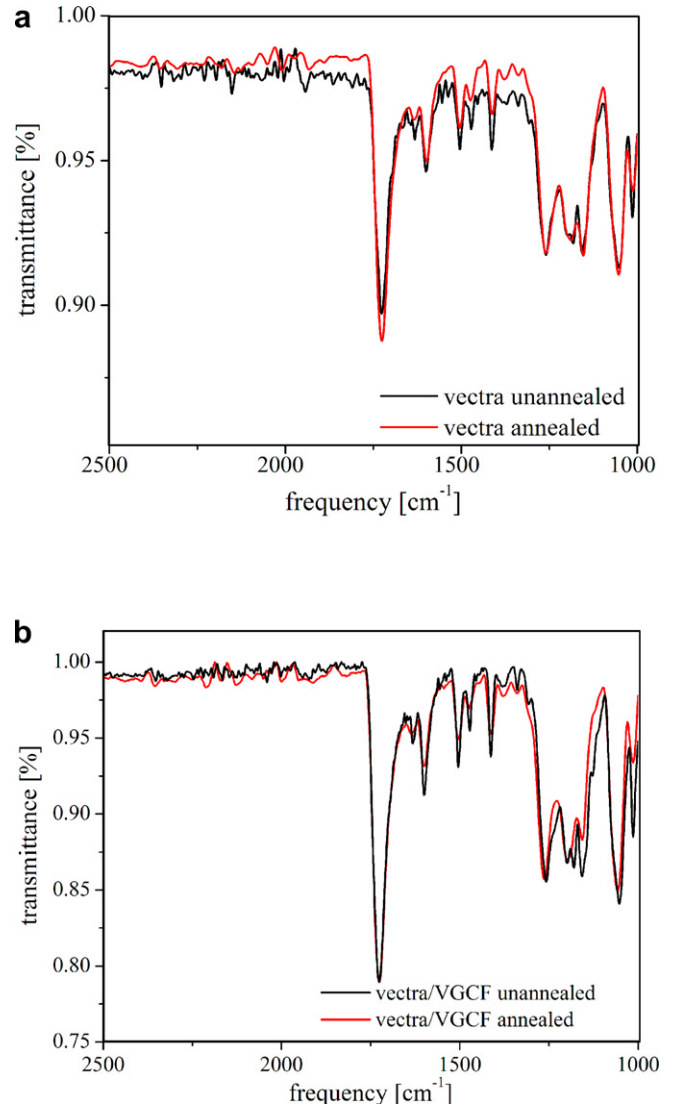


**Fig. 9.** FTIR spectra of (a) vectra and (b) vectra/VGCF with DD = 5 before and after annealing 120 min at 240 °C.

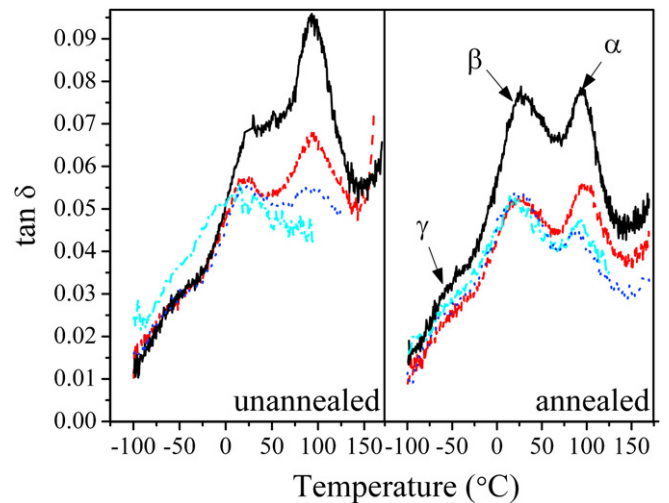


**Fig. 10.** Annealing (120 min at 240 °C) and DD effect on tan  $\delta$  traces in vectra/VGCF for (—) DD = 1.65, (---) DD = 36, (...) DD = 100 and (-.-) DD = 225.

**Table 2**

Annealing effect (120 min at 240 °C) on relaxation transition temperature (in °C) in vectra/VGCF. The relaxation temperatures were derived from the  $\tan \delta$  plot.

DD	Unannealed			Annealed		
	$\gamma$	$\beta$	$\alpha$	$\gamma$	$\beta$	$\alpha$
1.65	-59	22	93	-56	28	95
36	-59	21	92	-55	26	97
100	-56	21	88	-51	25	91
225	-54	15	86	-50	19	91

more structured crystalline phase. In the particular case of nano-composites, inclusions such as VGCF can act as nucleating agents inducing crystallization of the polymer at the adjacent sites. However, the XRD analysis performed on the annealed monofilament did not show any significant changes in the diffraction patterns, and in particular showed no increase of the crystalline fraction. Thus we can exclude the possibility of a recrystallization process induced by CIR when the composite is annealed for a short time at temperatures well below the crystal-to-nematic transition temperature. Also, the possibility that the cooperative motion of the molecular chain via ester interchange is disturbed by the presence of VGCF can be rejected on the basis of the DSC and the FTIR results.

A plausible explanation for the appearance of the new phase is a conformational rearrangement into reorganized domains within the copolymer (the PCL model), according to the model proposed by Schneggenburger [6]. Upon annealing of the drawn polymer, the un-oriented amorphous fraction is more mobile. In these domains, entropy driven translations of polymer chains tend to match similar conformational sequences (of HBA and HNA moieties) to form organized and ordered regions that solidify when the polymer is cooled to room temperature. The shift to higher temperatures observed in the  $\beta$  and  $\gamma$  transitions is in accordance with the sequential reorganization model suggested previously [6,10]. However, at this point, we have no explanation to the lowering of the  $\alpha$  and  $\beta$  transitions observed when DD is increased (although this is partially consistent with the proposed reorganization model).

To support the reorganization hypothesis, the formation of conformational reorganized domains was evaluated by  $^{13}\text{C}$  CP-MAS NMR spectroscopy [6,7], discriminating between the amorphous and crystalline phases on the basis of their respective relaxation times. The spectra obtained in the as-prepared vectra/VGCF, and after annealing at 240 °C, are displayed in Fig. 11. The relative area of the HNA and HBA ether ring carbon peaks, at 151 ppm and 155 ppm, respectively, reflects the composition of the ordered domains in the poly(HBA/HNA) [6], expressed as %-HNA. This ratio increases from 15% to 24% when DD increases from 1.65 to 100 in vectra/VGCF monofilament. Isometric annealing leads to an apparent reduction of the HNA ratio from 15% to 13% at DD = 1.65. This implies that HNA moieties are less affected by the reorganization process, most likely due to their lower concentration in the polymer. Assuming that this NMR analysis refers to the total oriented phase (crystalline and nematic) and applying the WAXD based calculation [23], the overall fraction of oriented phase in the drawn filament can be calculated. The WAXD results show that in the undrawn filament, 27% of the

**Table 3**

Annealing effect (120 min at 240 °C) on relaxation intensities (in a.u.) in vectra/VGCF. The relaxation intensities were derived from the  $\tan \delta$  plot.

DD	Unannealed			Annealed		
	$\gamma$	$\beta$	$\alpha$	$\gamma$	$\beta$	$\alpha$
1.65	0.033	0.067	0.093	0.035	0.077	0.076
36	0.026	0.057	0.066	0.025	0.052	0.055
100	0.028	0.055	0.055	0.025	0.050	0.045
225	0.035	0.054	0.052	0.029	0.053	0.049

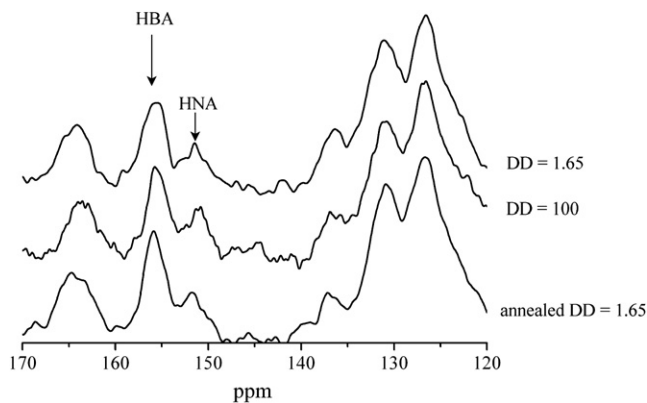


**Fig. 11.**  $^{13}\text{C}$  CP-MAS NMR spectra obtained for unannealed vectra with DD = 1.65 and DD = 100 and annealed (120 min at 240 °C) vectra with DD = 1.65. The arrows indicate well resolved monomer peaks; the aromatic ring-ether carbons, at 155 and 151 ppm, allowed easy composition determination.

polymer is oriented while in a drawn filament (DD = 100), the oriented phase is approximately 59%. Considering the assumption that in the specific case of nematic copolymer, the classical notion of crystallinity is replaced by the notion of order and orientation, the fraction of ordered HNA in the overall polymer can be evaluated. It shows a significant increase after drawing (from 4% at DD = 1.65–14% at DD = 100) but remains unchanged after annealing (4% at DD = 1.65). Concomitantly, the fraction of ordered HBA in the overall polymer is increased upon drawing (from 23% at DD = 1.65–45% at DD = 100) and annealing (from 23% to 33% at DD = 1.65). The evidence of increasing order in stretched filaments points to the role of amorphous disentanglements in the ordering process. Combining the NMR results with the relaxation transition results we can conclude that during the annealing process, vitrification of HBA-rich sequences takes place, responsible for the new endotherm displayed in the DSC data. Simultaneously, the HNA sequence is displaced from the ordered phase to the amorphous phase. This can explain the increase of the  $\beta$  relaxation intensity observed after annealing.

## 5. Conclusion

The main conclusion of this study is that inherent to the nano-morphology of thermotropic liquid crystalline polymers is an unstable phase that is highly sensitive to annealing and drawing conditions. XRD analysis revealed no significant changes in the crystalline structure, rejecting the hypothesis of recrystallization during the annealing process. However, the mechanical properties of the filaments, both filled and unfilled, are improved by more than 20% after the annealing process. Finally, the DMTA results show significant differences in the annealed materials in terms of intensity and localization of the loss tangent peaks. Particularly, the HNA and HBA relative motions were shifted to higher temperatures while the intensity of the HNA motion was increased. Based on DMTA and  $^{13}\text{C}$  NMR results, the influence of DD and annealing on the morphological reorganization, results in a model based on entropy driven translations of polymer chains tending to form organized and ordered HBA-rich regions.

## References

- [1] Han H, Bhowmik PK. *Prog Polym Sci* 1997;22(7):1431–502.
- [2] Chung TS. *Polym Eng Sci* 1986;26(13):901–19. doi:10.1002/pen.760261302.
- [3] Hanna S, Ruomo-Urbe A, Windle AH. *Nature* 1993;366(6455):546–9. doi:10.1038/366546a0.
- [4] Biswas A, Blackwell J. *Macromolecules* 1988;21(11):3158–64. doi:10.1021/ma00189a006.

- [5] Biswas A, Blackwell J. *Macromolecules* 1988;21(11):3152–8. doi:10.1021/ma00189a005.
- [6] Schneggenburger LA, Osenar P, Economy J. *Macromolecules* 1997;30(13):3754–8. doi:10.1021/ma961900w.
- [7] Gentzler M, Reimer JA. *Macromolecules* 1997;30(29):8365–74. doi:10.1021/ma961109n.
- [8] Sarlin J, Tormala P. *J Polym Sci Part B-Polym Phys* 1991;29(4):395–405. doi:10.1002/polb.1991.090290402.
- [9] Sarlin J, Tormala P. *J Appl Polym Sci* 1993;50(7):1225–31. doi:10.1002/app.1993.070500713.
- [10] Kaito A, Kyotani M, Nakayama K. *Macromolecules* 1990;23:1035–40. doi:10.1021/ma00206a021.
- [11] Liu J, Rybnikar F, Geil PH. *J Macromol Sci Part B Phys* 1996;35(3 & 4):375–410. doi:10.1080/00222349608220386.
- [12] Lenz RW, Martin E, Schuler AN. *J Polym Sci Polym Chem* 1973;11(9):2265–71. doi:10.1002/pol.1973.170110916.
- [13] Lenz RW, Jin J, Feichtinger KA. *Polymer* 1983;24(3):327–34. doi:10.1016/0032-3861(83)90272-0.
- [14] Chen G, Lenz RW. *Polymer* 1985;26(9):1307–11. doi:10.1016/0032-3861(85)90304-0.
- [15] Lenz RW, Ohata K, Funt J. *J Polym Sci Polym Chem* 1973;11(9):2273–85. doi:10.1002/pol.1973.170110917.
- [16] Lenz RW, Go S. *J Polym Sci Polym Chem* 1973;11(11):2927–46. doi:10.1002/pol.1973.170111113.
- [17] Lenz RW, Go S. *J Polym Sci Polym Chem* 1974;12(1):1–10. doi:10.1002/pol.1974.170120101.
- [18] Flint AJ, Jaffe MJ, Haider I, DiBiaise JJ, Cornetta E. USPTO, patent number 5,945,216; 1999.
- [19] Jaffe M. *Encyclopedia Polym Sci Eng* 1987;7:699.
- [20] Kalfon-Cohen E, Wachtel E, Marom G, Pegoretti A. *Polymer* 2009;50(7):1797–804. doi:10.1016/j.polymer.2009.02.002.
- [21] Smirnova VE, Gofman IV, Yudin VE, Dobrovolskaya IP, Shumakov AN, Didenko AL, et al. *Polym Eng Sci* 2008;49(2):217–22. doi:10.1002/pol.934.
- [22] Yoon HN, Charbonneau LF, Clundann GW. *Adv Mater* 1992;4(3):206–14. doi:10.1002/adma.19920040311.
- [23] Bassett DC, Olley RH. *Polymer* 1984;25(7). doi:10.1016/0032-3861(84)90076-4. 935–743.
- [24] Roe RJ. *Methods for X-ray and neutron scattering in polymer science*. England: Oxford University Press; 2000.
- [25] Hanna S, Lemmon TJ, Spontak RJ, Windle AH. *Polymer* 1992;33(1):3–10. doi:10.1016/0032-3861(92)90552-8.
- [26] Kalfon-Cohen E, Wachtel E, Marom G, Pegoretti A, Migliaresi C. *Polym Adv Technol* 2007;18(9):771–9. doi:10.1002/pol.934.
- [27] Taylor JE, Romo-Urbe A, Libera MR. *Polym Adv Technol* 2003;14(9):595–600. doi:10.1002/pol.374.
- [28] Kaito A, Kyotani M, Nakayama K. *J Macromol Sci Phys* 1995;B34(1–2):105–18.
- [29] Kalika DS, Yoon DY. *Macromolecules* 1991;24(11):3404–12. doi:10.1021/ma00011a057.
- [30] Mc Crum NG, Read BE, William G. *Unelastic and dielectric effect in polymeric solids*. Wiley, London, 1967. New York: Republished Dover; 1991.
- [31] Avakian P, Coburn JC, Conolly MS, Sauer BB. *Polymer* 1996;37(17):3843–50. doi:10.1016/0032-3861(96)00218-2.
- [32] Wellman MW, Adams WW, Wolff RA, Dudis DS, Wiff DR, Fratini AV. *Macromolecules* 1981;14(4):935–9. doi:10.1021/ma50005a009.
- [33] Troughton MJ, Davies GR, Ward IM. *Polymer* 1989;30(1):58–62. doi:10.1016/0032-3861(89)90383-2.